/
Article / Book Information

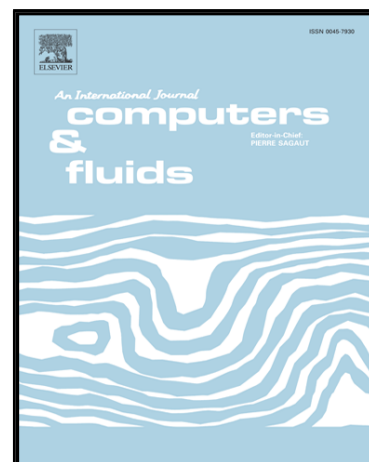|	
Title	Cholesky decomposition-based generation of artificial inflow turbulence including scalar fluctuation
Authors	Tsubasa Okaze, Akashi Mochida
Citation	Computers & Fluids, Vol. 159, pp. 23-32
Pub. date	2017, 12
DOI	http://dx.doi.org/10.1016/j.compfluid.2017.09.005
Note	This file is author (final) version.
Creative Commons	See next page.

License

Accepted Manuscript

Cholesky decomposition–based generation of artificial inflow turbulence including scalar fluctuation

T. Okaze , A. Mochida

Please cite this article as: T. Okaze , A. Mochida , Cholesky decomposition–based generation of artificial inflow turbulence including scalar fluctuation, *Computers and Fluids* (2017), doi: 10.1016/j.compfluid.2017.09.005

Highlights

- An artificial turbulence generation method including scalar fluctuation was proposed.

- This method is based on the Cholesky decomposition of turbulence flux tensors.

- We performed an LES with generated inflow turbulence in a half-channel.

Cholesky decomposition–based generation of artificial inflow turbulence including scalar fluctuation

T. Okaze[a*], A. Mochida[b]

[a]*Tokyo Institute of Technology, Yokohama, Japan*

[b]*Tohoku University, Sendai, Japan*

ABSTRACT: This paper proposes a new method for generating turbulent fluctuations in wind velocity and scalars, such as temperature and contaminant concentration, based on a Cholesky decomposition of the time-averaged turbulent flux tensors of the momentum and the scalar for inflow boundary condition of large-eddy simulation (LES). The artificial turbulent fluctuations generated by this method satisfy not only the prescribed profiles for the turbulent fluxes of the momentum and the scalar but also the prescribed spatial and time correlations. Based on an existing method that is able to impose the spatial and time correlations using digital filters, random two-dimensional data are filtered to generate a set of two-dimensional data with the prescribed spatial correlation. Then, these data are combined with those from the previous time step by using two weighting factors based on an exponential function. The method was validated by applying generated inflow turbulence to an LES computation of contaminant dispersion in a half-channel flow.

Keywords: Artificial turbulence generation, Inflow boundary condition, Large-eddy simulation, Space correlation, Time correlation, Cholesky decomposition

---

* Corresponding author. Tel.: +81-45- 924-5576
  E-mail address: okaze.t.aa@m.titech.ac.jp (T. Okaze).

1 INTRODUCTION

Computational fluid dynamics (CFD) is widely used in the field of computational wind engineering to predict urban wind environments [1,2]. Most attempts have utilized turbulence models based on the Reynolds-averaged Navier–Stokes equations [1,3–5]. In recent years, the growth of computing power makes it possible to apply large-eddy simulation (LES) to urban areas. One of the biggest unresolved issues involves the generation of inflow turbulence that reproduces upstream flow conditions. It is known that inflow turbulence properties greatly affect the flow field around buildings [6–8]. This means that time-dependent inflow turbulence within the atmospheric boundary layer should be well reproduced not only for the turbulence statistics but also for the instantaneous turbulent structures.

Various inflow generating methods have been proposed, as reviewed in detail by Tabor and Ahamadi [9] and Wu [10]. According to Wu [10], these techniques for generating inflow turbulence can be classified into two categories: recycling methods and synthetic methods. Recycling methods consist of strong recycling methods, which are based on recycling simulation [11,12], and weak recycling methods, which are based on rescaling–recycling simulation [13,14]. Recycling methods store the time history of velocity fluctuations obtained from a recycling CFD computation conducted as a preliminary simulation. The weak recycling methods proposed by Lund et al. [14] and Kataoka and Mizuno [15] have been widely used to generate fully developed atmospheric boundary layers used as inflow boundary condition for LES around buildings.

In contrast, synthetic methods artificially generate inflow turbulence with prescribed turbulence statistics using random numbers without conducting CFD computations. An advantage of the synthetic methods is that they do not require preliminary simulation of the flow field to obtain the fluctuations used as the inflow boundary condition of the main simulation. Hence, the total computational cost is reduced compared to recycling methods.

As shown by Wu [10], the synthetic methods mainly consist of four approaches: 1) synthetic random Fourier methods (SRFMs), which are based on inverse Fourier transforms of prescribed power spectra and cross spectra [16–19], 2) synthetic digital filter methods (SDFMs), which are based on the convolution of random numbers with a spatial digital-filter [20–23], 3) synthetic coherent eddy methods (SCEMs), which are based on the superposition of a large number of convected eddies [24,25], and 4) synthetic volume forcing methods (SVFMs), which are based on the addition of synthetic body force terms to the Navier–Stokes equations [26,27].

SRFM is a pioneering technique for synthetic methods. Lee et al. [16] proposed an SRFM that uses the inverse Fourier transform and satisfied the prescribed power spectrum for homogeneous isotopic turbulence. Then, a spatially decaying turbulence simulation was performed using the artificially generated homogeneous isotopic turbulence. Because the synthetic fluctuations are calculated independently, the Reynolds stress will be zero. Le and Moin [28,29] revised Lee et al.'s SRFM [16] for wall-bounded flows in which the distributions of Reynolds stress should be considered based on a coordinate transformation of the generated synthetic fluctuations, and performed a direct numerical simulation (DNS) of the flow field over a backward-facing step with generated anisotropic turbulence as the inflow boundary condition. The summary of the transformation with Cholesky decomposition of the Reynolds stresses tensor matrix is introduced in the appendix of Lund et al. [14] and briefly described below. The values of wind velocity, u_i, are divided into the time-averaged values of u_i, $\langle u_i \rangle$, and the deviation from the time-averaged value, u_i':

$$u_i = \langle u_i \rangle + u_i'. \tag{1}$$

With the lower triangular matrix of the Reynolds stress tensor matrix, a_{ij}, and a variable, Ψ_j, satisfying $\langle \Psi_j \rangle = 0$ and $\langle \Psi_i \Psi_j \rangle = \delta_{ij}$, instantaneous wind velocity, u_i, that mathematically satisfy the prescribed Reynolds stresses can be generated as

4

$$u_i = \langle u_i \rangle + u_i' = \langle u_i \rangle + a_{ij}\Psi_j . \tag{2}$$

The mathematical theory suggests any Ψ_j can be chosen so long as it satisfies $\langle \Psi_j \rangle = 0$ and $\langle \Psi_i \Psi_j \rangle = \delta_{ij}$. This transformation was immediately recognized. Then, SDFMs and SCEMs were developed to generate Ψ_j satisfying not only the prescribed Reynolds stresses but also spatial and time correlations.

Jarrin et al. [24] developed an SCEM that calculates Ψ_j as the superposition of a large number of eddies within a length scale related to the turbulence integral length scale. Klein et al. [20] proposed a SDFM in which Ψ_j are defined as a three dimensional convolution of random numbers with a digital filter to impose space correlation. Xie and Castro [21] revised and simplified Klein et al.'s approach [20] to efficiently generate an inflow turbulence with a two dimensional digital filter and demonstrated LES over a building array. This method imposes space correlations on the wind velocity fluctuations of the lateral and vertical directions and time correlations on those of the streamwise direction.

Almost simultaneously, Spille-Kohoff and Kaltenbach [26] proposed a SVFM and demonstrated a spatially developing turbulent boundary layer similar to that of Lund et al. [14]. In this method, direct forcing terms added in the Navier–Stokes equations are applied in a control zone adjacent to the inlet boundary to achieve a prescribed Reynolds stress distribution. The instantaneous body force is computed with a PI controller as a function of the error signal, which is the difference between the current time step and the prescribed values.

In recent years, several non-isothermal LES computations within urban boundary layers have been performed [30–33]. When LES is applied to a non-isothermal flow-field, both the inflow velocity fluctuation and the air temperature fluctuation should be reproduced. Only a few inflow generation methods for wind velocity and air temperature fluctuations have been

proposed.

Kong et al. [34] proposed a generation method for inflow fluctuations of wind velocity and air temperature using Lund et al.'s method [14] according to the same rescaling and recycling law between air temperature and streamwise velocity. Hattori and Nagano [35] conducted DNSs for very weak stable and unstable boundary layers with the inflow turbulent fluctuations of wind velocity and air temperature generated by the method proposed by Kong et al. [34]. Jiang et al. [36] carried out LESs for weak stable and unstable boundary layers with the inflow turbulence including air temperature fluctuation generated by extending Kataoka's weak recycling method [15]. Tamura et al. [31] conducted a non-isothermal LES of the Tokyo metropolitan area with an inflow turbulence including air temperature fluctuation. They set up a driver region that consists of two domains in the preliminary calculation to generate inflow turbulence with the temperature fluctuation. In the first domain, a fully developed isothermal boundary layer over a rough wall was calculated with the recycling method by Lund et al. [14]. Then, in the second domain, a stable boundary layer simulated as a sea breeze was calculated using turbulent fluctuations stored from the calculation in the first domain as the inflow boundary condition and stored histories of the wind and the temperature fluctuations at the outlet boundary for the main simulation. Yoshie et al. [30] performed a preliminary LES in which the approaching section of heated roughness elements in a wind tunnel was completely reproduced and predicted gas dispersion around a high-rise building under an unstable stratification condition. Mirocha et al. [37] proposed a synthetic inflow-generation-method for nested LES from meso-scale flow predicted with a meso-scale meteorological model based on the concept of SVFM because the meso-scale flow includes essentially no resolved turbulent fluctuations. Forcing terms were added to the momentum equations for the horizontal directions and the transport equations for potential temperature to provide minimal disturbance to the flow field so

turbulence could develop naturally within the nested LES domain near the inflow boundaries. Muñoz-Esparza et al. [38,39] developed several perturbation generation methods for potential temperature with the forcing method to accelerate the generation of turbulence on nested LES inflow boundaries.

However, generation methods for wind velocity and air temperature fluctuations based on preliminary or subsequent calculations require additional computational costs. Furthermore, in these methods, the distributions of mean wind velocity and air temperature and their fluctuations are obtained after the preliminary computation. This means it is difficult to impose the prescribed profiles of wind velocity and air temperature and the turbulence fluxes of the momentum and air temperature. Synthetic methods using forcing terms require optimization of the location of the control zone and the parameters in the forcing terms. Thus, the process of the trial and error is usually needed for the current inflow generation methods.

This paper proposes a new method of artificially generating turbulent fluctuations in wind velocity and a scalar, such as air temperature and concentration, based on a simultaneous Cholesky decomposition of the time-averaged turbulence flux tensors of the momentum and the scalar. The artificial turbulent fluctuations generated using this method satisfy not only the prescribed profiles for the turbulence fluxes of the momentum and the scalar but also the prescribed spatial and time correlations. According to the method proposed by Xie and Castro [21], two-dimensional random data are filtered to generate a set of two-dimensional data with the prescribed spatial correlation. Then, these data are combined with those from the previous time step by using two weighting factors based on an exponential function corresponding to a time correlation of the fluctuations. The method was validated by applying the generated turbulent fluctuations to the inflow boundary conditions of an LES computation of contaminant dispersion without buoyancy in a half-channel flow.

2 NEW METHOD OF GENERATING INFLOW TURBULENCE INCLUDING SCALAR FLUCTUATION

In this study, we express the values of wind velocity and the scalar as f_i, the time-averaged values of f_i as $\langle f_i \rangle$, and the deviation from the time-averaged value as f_i':

$$f_i = \langle f_i \rangle + f_i', \tag{3}$$

where the subscripts $i = 1, 2, 3$ indicate the wind velocity components in the streamwise, lateral, and vertical directions (u, v, w), respectively, and $i = 4$ indicates the scalar value, ϕ. A regular matrix of the turbulence fluxes of the momentum and the scalar, R_{ij}, is defined as

$$R_{ij} = \begin{pmatrix} \langle u'u' \rangle & \langle u'v' \rangle & \langle u'w' \rangle & \langle u'\phi' \rangle \\ \langle v'u' \rangle & \langle v'v' \rangle & \langle v'w' \rangle & \langle v'\phi' \rangle \\ \langle w'u' \rangle & \langle w'v' \rangle & \langle w'w' \rangle & \langle w'\phi' \rangle \\ \langle \phi'u' \rangle & \langle \phi'v' \rangle & \langle \phi'w' \rangle & \langle \phi'\phi' \rangle \end{pmatrix}. \tag{4}$$

If we implement the Cholesky decomposition of R_{ij}, we obtain a lower triangular matrix, a_{ij}:

$$a_{ij} = \begin{pmatrix} \sqrt{R_{11}} & 0 & 0 & 0 \\ R_{21}/a_{11} & \sqrt{R_{22}-a_{21}^2} & 0 & 0 \\ R_{31}/a_{11} & R_{32}-a_{21}a_{31}/a_{22} & \sqrt{R_{33}-a_{31}^2-a_{32}^2} & 0 \\ R_{41}/a_{11} & R_{42}-a_{21}a_{41}/a_{22} & R_{43}-a_{31}a_{41}-a_{32}a_{42}/a_{33} & \sqrt{R_{44}-a_{41}^2-a_{42}^2-a_{43}^2} \end{pmatrix}. \tag{5}$$

With the lower triangular matrix a_{ij} and a variable Ψ_j satisfying $\langle \Psi_j \rangle = 0$ and $\langle \Psi_i \Psi_j \rangle = \delta_{ij}$, the fluctuations, f_i', can be rewritten as

$$f_i = \langle f_i \rangle + f_i' = \langle f_i \rangle + a_{ij}\Psi_j. \tag{6}$$

We extended the transformation originally proposed by Le and Moin [28,29] using the Reynolds stress tensor matrix to consider the turbulence fluxes of a scalar with a 4×4 matrix. The statistics obtained by using Eq. (6) mathematically satisfy the turbulence fluxes of the momentum and the scalar prescribed in Eq. (4).

To impose time and space correlations for each component of the fluctuations, the two-dimensional digital-filter method proposed by Xie and Castro [21] was employed as a brief

description shown below. The prescribed time and space correlations are assumed using exponential functions with an integral time scale, T, and a length scale, L:

$$\frac{\left\langle \Psi_j(t)\Psi_j(t+\tau)\right\rangle}{\left\langle \Psi_j(t)\Psi_j(t)\right\rangle} = \exp\left(-\frac{\pi\tau}{2T}\right), \tag{7}$$

$$\frac{\left\langle \Psi_j(r)\Psi_j(r+\lambda)\right\rangle}{\left\langle \Psi_j(r)\Psi_j(r)\right\rangle} = \exp\left(-\frac{\pi\lambda}{2L}\right). \tag{8}$$

The time advance for the artificially generated fluctuations on a grid point (m, n) is expressed as

$$\Psi_j(t+\Delta t, m, n) = \Psi_j(t, m, n)\exp\left(-\frac{\pi\Delta t}{2T}\right) + \psi_j(t, m, n)\left\{1-\exp\left(-\frac{\pi\Delta t}{T}\right)\right\}^{1/2}, \tag{9}$$

$$\psi_j(t, m, n) = \sum_{m'=-N_y}^{N_y}\sum_{n'=-N_z}^{N_z}b_{m'}b_{n'}r_{m+m',n+n'}, \tag{10}$$

where r is a random number satisfying $\langle r_j\rangle = 0$ and $\langle r_i r_j\rangle = \delta_{ij}$, b_k is a digital-filter coefficient for the integral length scale in the generated plane in each direction, and N_y and N_z are related to the length scale of the filter in each direction. Xie and Castro [21] recommended that $N \geq 2n$, where n is the number of grid points included in the integral length scale, so $N = 2n$ is used in this study. The filter coefficient is assumed in the form of an exponential function to impose the approximated space correlation with a simple solution by Klein et al. [20]:

$$b_k = \tilde{b}_k \Bigg/ \left(\sum_{j=-N}^{N}\tilde{b}_j^{\,2}\right)^{1/2}, \tag{11}$$

$$\tilde{b}_k = \exp\left(-\frac{\Delta x|k|}{L}\right). \tag{12}$$

By substituting ψ_j (as obtained using the new dataset of random numbers from Eqs. (10)–(12)) into Eq. (9) for each time step, Ψ_j for the next time step is calculated. Finally, the fluctuations, f_i', and instantaneous values of f_i are obtained by substituting Ψ_j into Eq. (6).

3 A PRIORI LES COMPUTATIONS

3.1 *Outline of computations*

A priori LES computations for a half-channel were carried out to validate the reproducibility of the flow and dispersion fields by applying the artificially generated wind and scalar fluctuations based on the proposed generation method as inflow boundary conditions. Fig. 1 shows a diagram of the computations.

First, a preliminary LES computation was conducted to obtain turbulence statistics in the fully developed half channel flow, as shown in Fig. 1(a). A line source was placed on the ground cell immediately behind the inflow boundary and a passive scalar was emitted. The emission rate of the passive scalar per unit time and unit area, q, was set to 1.0. The mean and turbulence statistics of the wind and scalar values were stored on the y-z plane at the center of the calculation domain.

Then, at the inlet of the main LES domain (Fig. 1(b)), the time histories of the wind and scalar values were artificially generated based on the Cholesky decomposition of the time-averaged turbulence flux tensor of the momentum and the scalar, which was obtained from the database collected at $x = 5.0H$ in the preliminary simulation.

Finally, the main LES computation was carried out with the artificially generated turbulent fluctuations as the inflow boundary conditions of the main computation. The reproducibility of the flow and dispersion fields when applying the artificially generated wind and scalar fluctuations as inflow boundary conditions was validated by comparing the results for the flow and the dispersion fields from $x = 0.0H$ to $5.0H$ in the main calculation with those obtained from $x = 5.0H$ to $10.0H$ in the preliminary calculation.

3.2 *Numerical settings*

The dimensions of the computational domain in both the preliminary and main simulations were $10.0H \times 1.0H \times 1.0H$ in the streamwise (x), lateral (y), and vertical (z) directions, respectively. The computational domain comprised $320 \times 32 \times 32$ cells with a uniform grid. A structural grid system was used. The Reynolds number, which was defined with the mean wind velocity at the top of the domain, U, and the domain height, H, was set to 3.2×10^4.

A second-order central difference scheme was used for the spatial discretization of all advection and diffusion terms in the governing equations. The second-order Adams–Bashforth scheme was used to discretize the time-dependent terms. The standard Smagorinsky model was applied to reproduce the subgrid-scale stress with a Smagorinsky constant of $C_s = 0.10$. The Schmitt number and the sub-grid scale Schmitt number were set to 1.0. An averaged pressure gradient was imposed in the streamwise direction as the driving force in the preliminary calculation to obtain the turbulence statistics in the fully developed half channel flow. The simplified marker and cell (SMAC) algorithm was applied to couple the equations for momentum and mass conservation in incompressible flow. The turbulence statistics for both simulations were collected and averaged over $\Delta T^* = 20$ after a sufficient initial calculation. The non-dimensional time, ΔT^*, is defined as $\Delta T^* = \Delta T \cdot \langle u^* \rangle / H$, where ΔT is the calculation time, $\langle u^* \rangle$ is the friction velocity on the surface of the ground and H is the domain height.

3.3 *Boundary conditions*

In the preliminary simulation, periodic boundary conditions were imposed in both the streamwise and lateral directions for the wind field to achieve fully developed flow field. An advective outlet condition was applied to the outlet boundary for the scalar field.

11

In the main simulation, artificially generated fluctuations based on the method proposed in Section 2 were used as the inflow boundary conditions of the wind and scalar field. The integral length scale for prescribing the space correlations of the turbulent fluctuations of wind velocity was assumed to be $L = 0.15H$ based on the results of a previous study [22] that examined the same situation of a half-channel simulation for investigating the effects of artificially generated fluctuations of the wind velocity components on a reproduced flow field. The integral time scale for prescribing the time correlations of the turbulent fluctuations is given based on the frozen turbulence approximation known as "Taylor's hypothesis of frozen turbulence":

$$T = L / U, \tag{11}$$

where U is the time- and space-averaged wind velocity at the upper boundary. It is assumed that the integral length and time scales for scalar dispersion are equal to those for the wind velocity; likewise, Xie et al. [40] assumed the same values for the integral length scales of the velocity and temperature at the inflow boundary. A periodic boundary condition was imposed only in the lateral direction of the flow and scalar fields. An advective outlet condition was applied to the outlet boundary for the flow and scalar fields.

Werner and Wengle's two-layer model [41] was adopted to estimate the shear stress on the ground surface by assuming linear and 1/7 power law distributions of the instantaneous velocity in both the preliminary and main simulations. A slip-wall boundary condition was imposed for the upper boundary condition in both simulations.

3.4 *Computational cases*

Three cases were carried out, as listed in Table 1. In Case-fluc, both the artificially generated fluctuations of the wind and the scalar were imposed as the inflow boundary condition of the main simulation. In contrast, in Case-mean, the artificially generated fluctuations of the wind velocity were imposed—similarly to Case-fluc—but the fluctuation of the scalar was not

generated. In this case, the artificially generated fluctuations of the wind velocity and the mean value of the scalar (without turbulent fluctuation) obtained from the preliminary simulation were employed. In addition, in Case-c2, both the artificially generated fluctuations of the wind and the scalar were also imposed. However, the inflow turbulence in Case-c2 was generated by only prescribing the Reynolds stresses and the variance of the scalar fluctuation from the preliminary LES. The cross-correlations of the wind and scalar fluctuations of the inflow turbulence in Case-2 were set to zero. This means that the artificial fluctuation of the scalar in Case-c2 was generated independently from the wind velocity fluctuations.

4 RESULTS AND DISCUSSION

4.1 *Turbulence statistics of generated fluctuations for wind and scalar*

Fig. 2 shows a comparison of the mean values and turbulence statistics between the target values obtained from the preliminary simulation and the artificially generated values based on the method proposed in Section 2. The generated mean wind velocity and concentration precisely agree with the target values. The variances of the generated streamwise component of the fluctuation of the wind velocity and the concentration are also in good agreement with the target values. In addition, the artificially generated turbulence fluxes—which are correlations between the turbulent fluctuations of the streamwise and vertical components of the wind velocity, the fluctuations of the wind velocity in each direction, and the fluctuation of the concentration—correspond to the turbulence fluxes from the target values. This confirms that the generated turbulent fluctuations in the wind and the scalar values, as obtained by this proposed method, satisfy the prescribed time-averaged turbulence flux tensors of the momentum and the scalar.

4.2 *Reproducibility of flow field with artificially generated inflow boundary conditions*

Fig. 3 shows the streamwise change in the vertical distributions of the turbulence statistics for the flow field. The mean wind velocity changes very little in the downstream region, which is in good agreement with the target value obtained from the preliminary simulation. The turbulence kinetic energy in the grid scale at $x = 1.0H$ (just leeward of the inflow boundary) is strongly damped by 40%, relative to the target value. Previous researchers [21,42] have suspected that the causes are related to the artificially generated fluctuations not generally being able to satisfy the continuity and momentum equations, as the generated fluctuations database does not include pressure fluctuations. The turbulence kinetic energy near the surface more closely approaches the target value as the flow moves downstream owing to the reproduction of the turbulence kinetic energy by the gradient of the mean wind velocity near the surface. In Fig. 3(c), the variance of the streamwise component of the wind velocity fluctuation is reduced by 40% at $x = 1.0H$, but it increases as the flow moves downstream. This streamwise change is similar to that of the turbulence kinetic energy. In contrast, in Fig. 3(d), the variance in the vertical component of the wind velocity fluctuation drastically undershoots the target value at $x = 1.0H$, especially near the surface. One of the reasons for this reduction of the vertical component of the wind velocity fluctuation is thought to be that both the integral length scales in the streamwise and vertical directions are set to the same value.

Fig. 4 shows the streamwise change of the friction velocity on the ground surface normalized with the friction velocity in the preliminary simulation. The friction velocity decreased by 5% aroud $x = 1.0H$; however, the vertical profiles of the mean wind did not change along with the streamwise direction, as shown Fig. 3(a). This decreasing of the friction velocity was caused by damping of the turbulence kinetic energy immediately behind the inflow boundary. The friction velocity increased depending on the regeneration of

turbulent fluctuation near the surface. The friction velocity in the main simulation reached that in the preliminary simulation near $x = 4.0H$.

4.3 *Reproducibility of dispersion field with artificially generated fluctuation of scalar at inflow boundary*

Fig. 5 compares the streamwise changes in the vertical distribution of the mean concentration $\langle c \rangle$. The result of the mean concentration obtained from the main simulation with artificially generated fluctuations in Case-fluc was slightly larger than the result of the preliminary simulation near the surface. This difference is attributed to the underestimation of the turbulent diffusion of the passive scalar in the upward area, which is due to the damping of the turbulence kinetic energy near the inflow boundary. The mean concentrations in Case-mean and Case-c2 were larger than those in both the preliminary simulation and Case-fluc, especially near the ground surface. In Case-mean and Case-c2, the cross-correlations between the wind velocity and scalar fluctuations were not imposed. This led to the underestimation of the turbulence fluxes of the scalar in the vertical direction. Consequently, the mean concentrations near the ground increased in Case-mean and Case-c2.

The streamwise change in the vertical distributions of the turbulence flux of the passive scalar for the vertical component $\langle w'c' \rangle$ is shown in Fig. 6. The heights of the peak values of $\langle w'c' \rangle$ for three cases are observed at the same position, and they correspond to that in the preliminary simulation at each sampled line. The fluxes near the ground surface in three cases increase at $x = 3.0H$ and $5.0H$ with the increase in the turbulence kinetic energy near the ground. The turbulence flux in Case-fluc at $x = 1.0H$ also agreed well with that in the preliminary LES; in contrast, the fluxes in Case-mean and Case-c2 underestimated it owing to the lack of turbulence fluxes of the scalar at the inflow boundary.

Fig. 7 shows the streamwise change in the vertical distribution of the variance of the passive scalar fluctuation $\langle c'^2 \rangle$. The results in Case-fluc were somewhat overestimated for each line, but the distribution profile and the height at which the peak value of $\langle c'^2 \rangle$ appears are similar to the results obtained with the preliminary simulation. The underestimation of $\langle w'c' \rangle$, mentioned above, leads to poor turbulent diffusion, and the high windward concentrations would trend to the leeward side. As a result, $\langle c'^2 \rangle$ was overestimated in the main simulation. The results in Case-mean showed smaller values than the preliminary simulation in all lines. Especially, $\langle c'^2 \rangle$ at $x = 1.0H$ in Case-mean was underestimated because scalar fluctuation was not imposed. The streamwise change of $\langle c'^2 \rangle$ in Case-c2 was roughly similar to that in the preliminary LES and Case-fluc. However, $\langle c'^2 \rangle$ at $x = 5.0H$ in Case-c2 was slightly larger than that in the preliminary LES and Case-fluc. This means that even at $x = 5.0H$, the concentrations in Case-c2 continued to be higher or lower than those in the respective regions of Case-fluc because of the underestimation of $\langle w'c' \rangle$ in this region, which is caused by the lack of $\langle w'c' \rangle$ at the inflow boundary.

Fig. 8 shows the comparison of the streamwise changes of the mean concentration and the variance of the fluctuation of the concentration at $z = 0.1H$. The mean concentration decreased along the streamwise direction owing to the scalar diffusion in the vertical direction. The mean concentrations in Case-mean and Case-c2 were 10% higher than that in Case-fluc. The decreasing trend of the concentration in Case-fluc was reproduced fairly well with that in the preliminary simulation. The concentrations in Case-mean and Case-c2 near $x = 1.0H$ were almost constant. This indicates that the turbulent diffusion did not well reproduce the preliminary behavior because the cross-correlation of the wind velocity and the scalar fluctuations were not considered in Case-mean and Case-c2. The variance of the concentration in Case-fluc, which decreased immediately behind the inflow boundary, approached that in the preliminary simulation as the flow moved downstream. In contrast, the

16

variance in Case-mean was completely different from that in the preliminary LES within $0.0H < x < 3.0H$. The variance in Case-mean was close to the preliminary result within the downstream region. However, the variance in Case-mean was still smaller than that in the preliminary result near $x = 5.0H$. By applying the artificially generated wind and scalar fluctuations as inflow boundary conditions, the dispersion field was well reproduced.

5 CONCLUSIONS

A new method for generating the turbulent fluctuations in the three components of wind velocity and scalar quantities, such as temperature and contaminant concentration, was developed based on the Cholesky decomposition of the time-averaged turbulence flux tensors of the momentum and the scalar. By employing a 5×5 non-singular matrix as a turbulence flux tensor matrix, the proposed method can generate the time series of wind velocity, temperature, and concentration of contaminants. This method can be applied to other synthetic methods based on the Cholesky decomposition of the Reynolds stresses such as the SCEM proposed by Jarrin et al. [24].

LES computations for a half-channel were carried out to validate the reproducibility of the flow and dispersion fields by applying the artificially generated wind and scalar fluctuations as inflow boundary conditions. The streamwise change in the mean concentration was reproduced accurately by means of the preliminary simulation. Although $\langle w'c' \rangle$ was underestimated and $\langle c'^2 \rangle$ was overestimated slightly owing to the damping of the turbulence kinetic energy, the dispersion field was well reproduced with the artificially generated wind and scalar fluctuations based on the proposed inflow boundary conditions compared to the simulation with the generated fluctuations of wind velocity only. The cross-correlations of wind velocity and scalar fluctuations imposed on the inflow turbulence greatly affected the turbulent diffusion of the passive scalar in the downstream area in this study. The lack of

cross-correlations between wind velocity and scalar fluctuations at the inflow boundary led to less turbulent diffusion of the scalar in the downstream region. When the proposed method is applied to practical situations, it is sometimes difficult to know the correct values for the cross-correlations of wind velocity and scalar fluctuations. To set the cross-correlations of wind velocity and scalar fluctuations, such as turbulence heat flux and turbulence concentration flux, several assumptions—i.e., the empirical relationship under thermal stratifications and the concept of the eddy-viscosity model with mean values—are needed. Further investigations of the applicability of this method to non-isothermal flow fields and the practicality of the proposed method with assumed cross-correlations of wind velocity and scalar fluctuations to LES in actual situations should be undertaken.

ACKNOWLEDGMENT

REFERENCES

[1]   Blocken B. 50 years of Computational Wind Engineering: Past, present and future. J Wind Eng Ind Aerodyn 2014;129:69–102. doi:10.1016/j.jweia.2014.03.008.

[2]   Blocken B. Computational Fluid Dynamics for urban physics: Importance, scales, possibilities, limitations and ten tips and tricks towards accurate and reliable simulations. Build Environ 2015;91:219–45.

[3]   Franke J, Hellsten A, Schatzmann M, Bertrand C. Best practice guideline for the CFD simulation offlows in the urban environment. COST Office Brussels; 2007.

[4]   Tominaga Y, Mochida A, Yoshie R, Kataoka H, Nozu T, Yoshikawa M, et al. AIJ guidelines for practical applications of CFD to pedestrian wind environment around buildings. J Wind Eng Ind Aerodyn 2008;96:1749–61. doi:10.1016/j.jweia.2008.02.058.

[5]   Architectual Institute of Japan. AIJ Benchmarks for Validation of CFD Simulations Applied to Pedestrian Wind Environment around Buildings. Architectual Institute of Japan; 2016.

[6]   Mochida A, Lun IYF. Prediction of wind environment and thermal comfort at pedestrian level in urban area. J Wind Eng Ind Aerodyn 2008;96:1498–527. doi:10.1016/j.jweia.2008.02.033.

[7]   Tamura T. Towards practical use of LES in wind engineering. J Wind Eng Ind Aerodyn 2008;96:1451–71. doi:10.1016/j.jweia.2008.02.034.

[8]   Yan BW, Li QS. Inflow turbulence generation methods with large eddy simulation for wind effects on tall buildings 2015. doi:10.1016/j.compfluid.2015.04.020.

[9]   Tabor GR, Baba-Ahmadi MH. Inlet conditions for large eddy simulation: A review. Comput Fluids 2010;39:553–67. doi:10.1016/j.compfluid.2009.10.007.

[10]   Wu X. Inflow Turbulence Generation Methods. Annu Rev Fluid Mech 2017;49:23–49. doi:10.1146/annurev-fluid-010816-060322.

[11]   Rogallo RS, Moin P. Numerical Simulation of Turbulent Flows. Annu Rev Fluid Mech 1984;16:99–137. doi:10.1146/annurev.fl.16.010184.000531.

[12]   Moin P, Mahesh K. DIRECT NUMERICAL SIMULATION: A Tool in Turbulence Research. Annu Rev Fluid Mech 1998;30:539–78. doi:10.1146/annurev.fluid.30.1.539.

[13]   Wu X, Squires KD, Lund TS. Large Eddy Simulation of a Spatially-Developing Boundary Layer. Supercomput 1995 Proc IEEE/ACM SC95 Conf 1995:1–18. doi:10.1109/SUPERC.1995.241964.

[14]   Lund TS, Wu X, Squires KD. Generation of Turbulent Inflow Data for Spatially-Developing Boundary Layer Simulations. J Comput Phys 1998;258:233–58.

[15]   Kataoka H, Mizuno M. Numerical flow computation around aeroelastic 3D square cylinder using inflow turbulence. Wind Struct 2002;5:379–92. doi:10.12989/was.2002.5.2_4.379.

[16]   Lee S, Lele SK, Moin P. Simulation of spatially evolving turbulence and the applicability of Taylor's hypothesis in compressible flow. Phys Fluids A Fluid Dyn 1992;4:1521–30. doi:10.1063/1.858425.

[17]   Kondo K, Murakami S, Mochida A. Generation of velocity fluctuations for inflow boundary condition of LES. J Wind Eng Ind Aerodyn 1997;67–68:51–64. doi:10.1016/S0167-6105(97)00062-7.

[18]   Iizuka S, Murakami S, Tsuchiya N., Mochida A. LES of flow past 2D cylinder with imposed inflow turbulence. Proc. 10th Int. Conf. Wind Eng., 1999, p. 1291–1298.

[19]   Kondo K, Tsuchiya M, Mochida A, Murakami S. Generation of inflow turbulent boundary layer for LES computation. Wind Struct 2002;5:209–26. doi:10.12989/was.2002.5.2_3_4.209.

[20]   Klein M, Sadiki A, Janicka J. A digital filter based generation of inflow data for spatially developing direct numerical or large eddy simulations. J Comput Phys 2003;186:652–65. doi:10.1016/S0021-9991(03)00090-1.

[21]   Xie Z-T, Castro IP. Efficient Generation of Inflow Conditions for Large Eddy Simulation of Street-Scale Flows. Flow, Turbul Combust 2008;81:449–70. doi:10.1007/s10494-008-9151-5.

[22]   Kondo A, Iizuka S. An Investigation of Artifical Genelation Methods of Inflow Turbulence for LES based on the Cholesky Decomposition of Reynolds Stresses. J Environ Eng (Transactions AIJ) 2012;77:661–9. doi:10.3130/aije.77.661.

[23]   Allegrini J, Carmeliet J. Evaluation of the Filtered Noise Turbulent Inflow Generation Method. Flow, Turbul Combust 2017;98:1087–115. doi:10.1007/s10494-016-9798-2.

[24]   Jarrin N, Benhamadouche S, Laurence D, Prosser R. A synthetic-eddy-method for generating inflow conditions for large-eddy simulations. Int J Heat Fluid Flow 2006;27:585–93. doi:10.1016/j.ijheatfluidflow.2006.02.006.

[25]   Jarrin N, Prosser R, Uribe J-C, Benhamadouche S, Laurence D. Reconstruction of turbulent fluctuations for hybrid RANS/LES simulations using a Synthetic-Eddy Method. Int J Heat Fluid Flow 2009;30:435–42. doi:10.1016/j.ijheatfluidflow.2009.02.016.

[26]   Spille-Kohoff A., Kaltenbach HJ. Generation of Turbulent Inflow Data with a Prescribed Shear-Stress Profile. Def Tech Inf Cent Compil Part Not 2001:ADP013648.

[27]   Mirocha J, Kosović B, Kirkil G, Mirocha J, Kosović B, Kirkil G. Resolved Turbulence Characteristics in Large-Eddy Simulations Nested within Mesoscale Simulations Using the Weather Research and Forecasting Model. Mon Weather Rev 2014;142:806–31. doi:10.1175/MWR-D-13-00064.1.

[28] Le H, Moin P. Direct numerical simulation of turbulent flow over a back-facing step. Rep TF-58, Thermosciences Div Stanford Univ 1994.

[29] LE H, MOIN P, KIM J. Direct numerical simulation of turbulent flow over a backward-facing step. J Fluid Mech 1997;330:S0022112096003941. doi:10.1017/S0022112096003941.

[30] Yoshie R, Jiang G, Shirasawa T, Chung J. CFD simulations of gas dispersion around high-rise building in non-isothermal boundary layer. J Wind Eng Ind Aerodyn 2011;99:279–88. doi:10.1016/j.jweia.2011.01.006.

[31] Tamura T, Nozu T, Okuda Y, Ohashi M, Umakawa H. Hybrid method of meteorological and LES models for heat environment. Proc. 8th Int. Conf. Urban Clim., 2012.

[32] Matsuda K, Onishi R, Yamada S, Yamato H, Ishikawa M, Takahashi K. Numerical analysis of heat environment in central Tokyo using tree-crown-resolving large-eddy simulation considering three-dimensional radiation process. 9th Int. Conf. Urban Clim., 2015.

[33] Yoshie R. Wind Tunnel Experiment and Large Eddy Simulation of Pollutant/Thermal Dispersion in Non-isothermal Turbulent Boundary Layer. Adv. Environ. Wind Eng., Tokyo: Springer Japan; 2016, p. 167–96. doi:10.1007/978-4-431-55912-2_9.

[34] Kong H, Choi H, Lee JS. Direct numerical simulation of turbulent thermal boundary layers. Phys Fluids 2000;12:2555. doi:10.1063/1.1287912.

[35] Hattori H, Houra T, Nagano Y. Direct numerical simulation of stable and unstable turbulent thermal boundary layers. Int J Heat Fluid Flow 2007;28:1262–71. doi:10.1016/j.ijheatfluidflow.2007.04.012.

22

[36]   Jiang G, Yoshie R, Shirasawa T, Jin X. Inflow turbulence generation for large eddy simulation in non-isothermal boundary layers. J Wind Eng Ind Aerodyn 2012;104–106:369–78. doi:10.1016/j.jweia.2012.02.030.

[37]   Mirocha J, Kosović B, Kirkil G. Resolved Turbulence Characteristics in Large-Eddy Simulations Nested within Mesoscale Simulations Using the Weather Research and Forecasting Model. Mon Weather Rev 2014;142:806–31. doi:10.1175/MWR-D-13-00064.1.

[38]   Muñoz-Esparza D, Kosovi B, Mirocha J, Van Beeck J, Muñoz-Esparza D, Van Beeck J, et al. Bridging the Transition from Mesoscale to Microscale Turbulence in Numerical Weather Prediction Models. Boundary-Layer Meteorol 2014;153:409–40. doi:10.1007/s10546-014-9956-9.

[39]   Muñoz-Esparza D, Kosović B, Van Beeck J, Mirocha J. A stochastic perturbation method to generate inflow turbulence in large- eddy simulation models: Application to neutrally stratified atmospheric boundary layers. Cit Phys Fluids 2015;27. doi:10.1063/1.4913572.

[40]   Xie Z-T, Hayden P, Wood CR. Large-eddy simulation of approaching-flow stratification on dispersion over arrays of buildings. Atmos Environ 2013;71:64–74. doi:10.1016/j.atmosenv.2013.01.054.

[41]   Werner H, Wengle H. Large-eddy simulation of turbulent flow over and around a cube in plate channel. Proc. 8th Symp. Turbul. Shear Flows, 1991, p. 155–8.

[42]   Dietzel D, Messig D, Piscaglia F, Montorfano A, Olenik G, Stein OT, et al. Evaluation of scale resolving turbulence generation methods for Large Eddy Simulation of turbulent flows. Comput Fluids 2014;93:116–28. doi:10.1016/j.compfluid.2014.01.013.

23

Periodic boundary condition only for flow field

10.0H

5.0H

Data storage plane

1.0H

z

x

Line source

The results were compared with those obtained from
x = 0.0H to x = 5.0H in the main LES.

(a) Preliminary LES

The inflow turbulence was artificially generated
from the turbulence statistics on the data storage plain of the preliminary LES.

z

x

The results were compared with those obtained from
x = 5.0H to x = 10.0H in the preliminary LES.

(b) Main LES

Fig. 1 Diagram of LES computations
  (a) Preliminary LES
  (b) Main LES

(a) $\langle u \rangle / U$
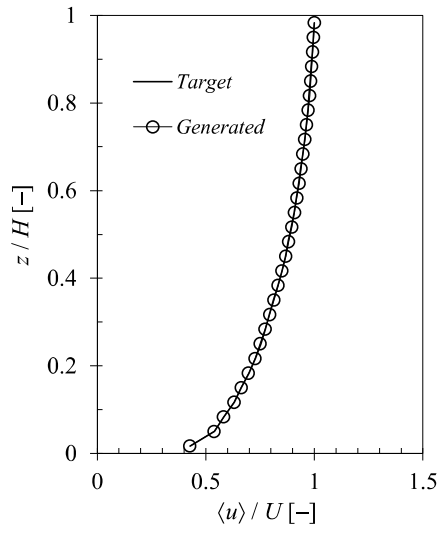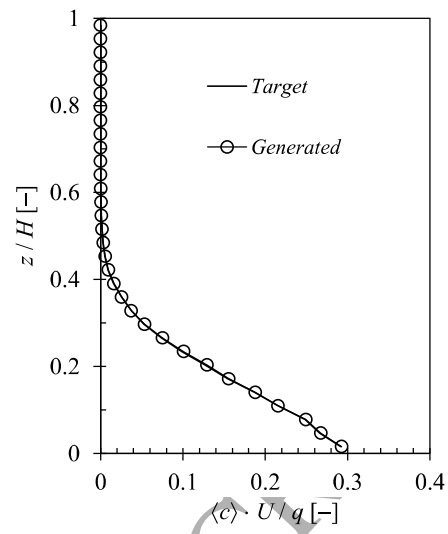
(b) $\langle c \rangle \cdot U / q$
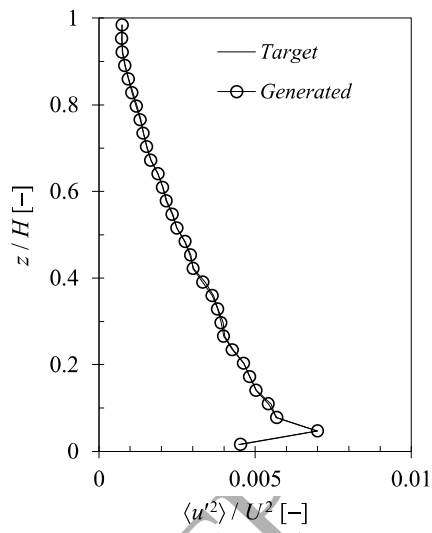
(c) $\langle u'^2 \rangle \cdot U^2$
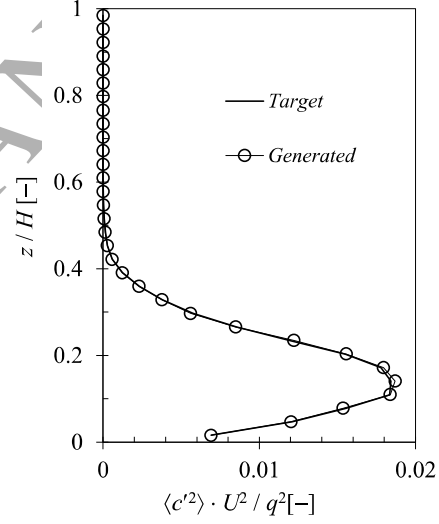
(d) $\langle c'^2 \rangle \cdot U^2 / q^2$
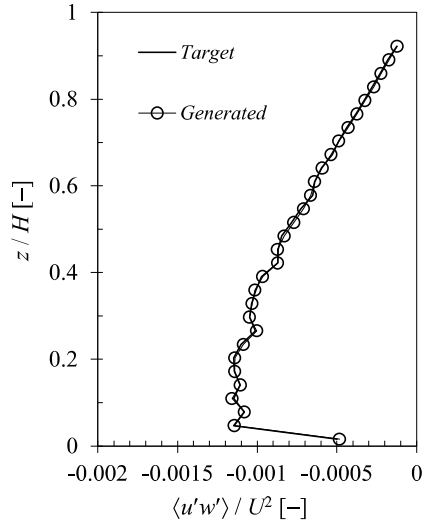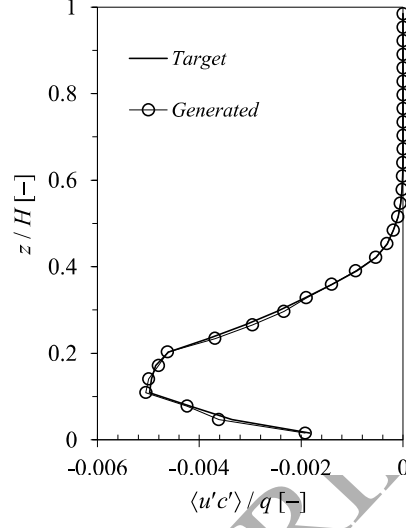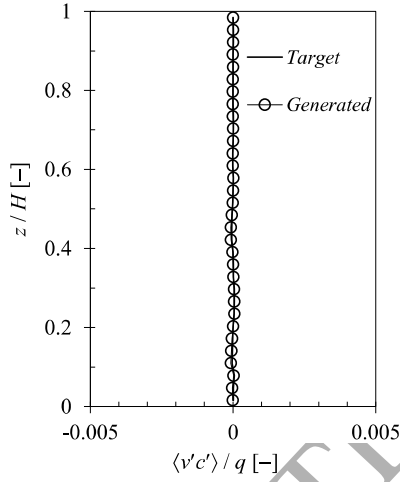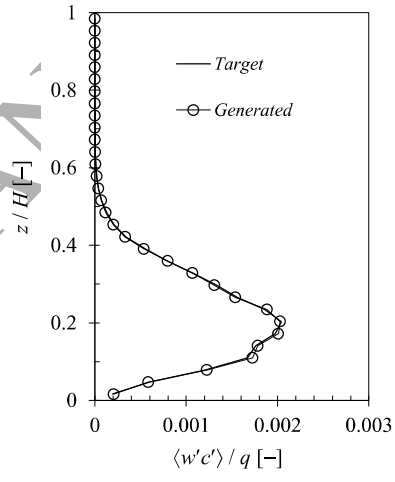
(e) $\langle u'w' \rangle / U^2$

(f) $\langle u'c' \rangle / q$

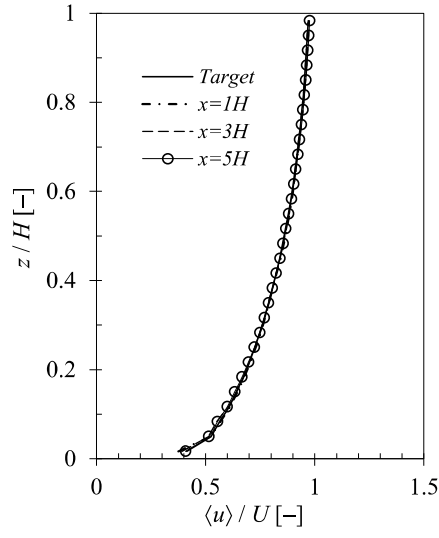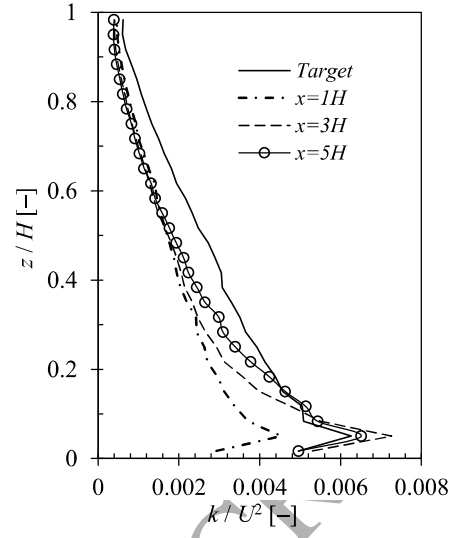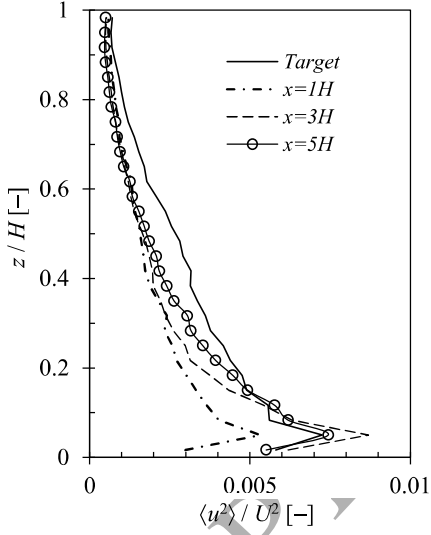(g) $\langle v'c' \rangle / q$
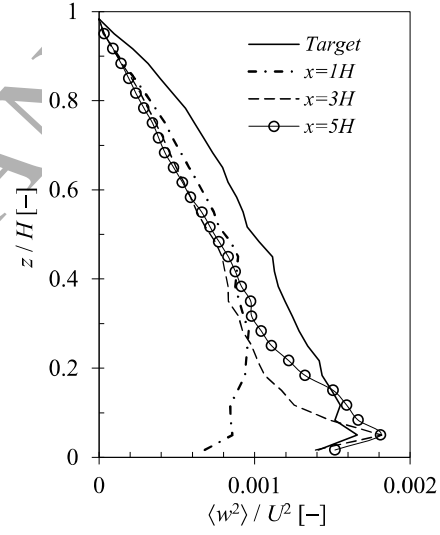

(h) $\langle w'c' \rangle / q$

Fig.2 Comparison of turbulence statistics for the target values obtained from the preliminary simulation and the artificially generated values based on the proposed method

(a) $\langle u \rangle / U$

(b) $\langle c \rangle \cdot U / q$

(c) $\langle u'^2 \rangle / U^2$

(d) $\langle c'^2 \rangle \cdot U^2 / q^2$

(e) $\langle u'w' \rangle / U^2$

(f) $\langle u'c' \rangle / q$

(g) $\langle v'c' \rangle / q$

(h) $\langle w'c' \rangle / q$

(a) $\langle u \rangle / U$

(b) k / U^2

(c) $\langle u'^2 \rangle / U^2$

(d) $\langle w'^2 \rangle / U^2$

Fig. 3 Streamwise change of vertical distribution in turbulence statistics for flow field

(a) $\langle u \rangle / U$

(b) k / U^2

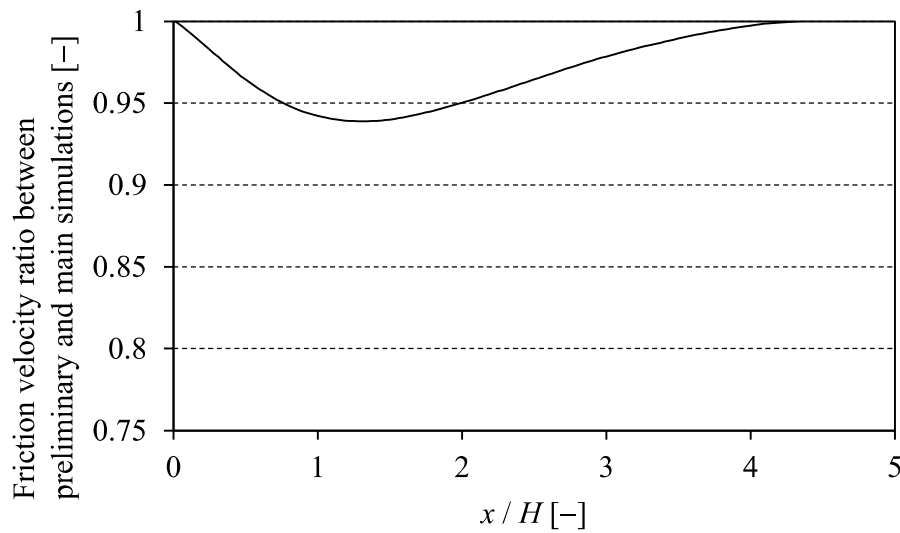(c) $\langle u'^2 \rangle / U^2$

(d) $\langle w'^2 \rangle / U^2$
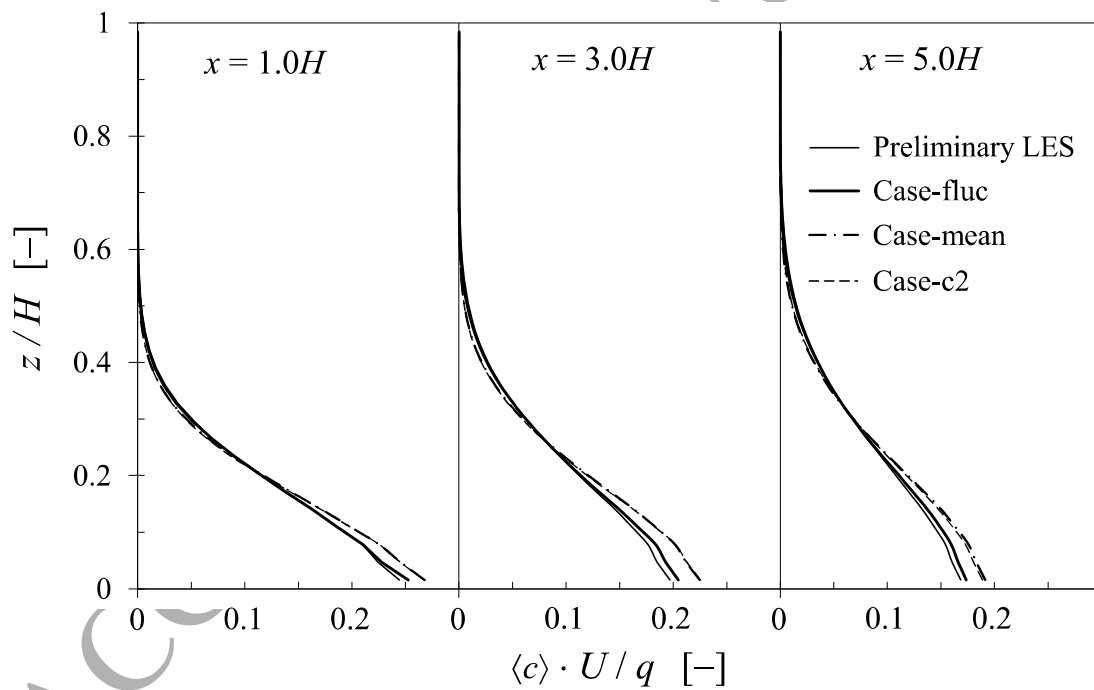
Fig. 4 Streamwise change of friction velocity

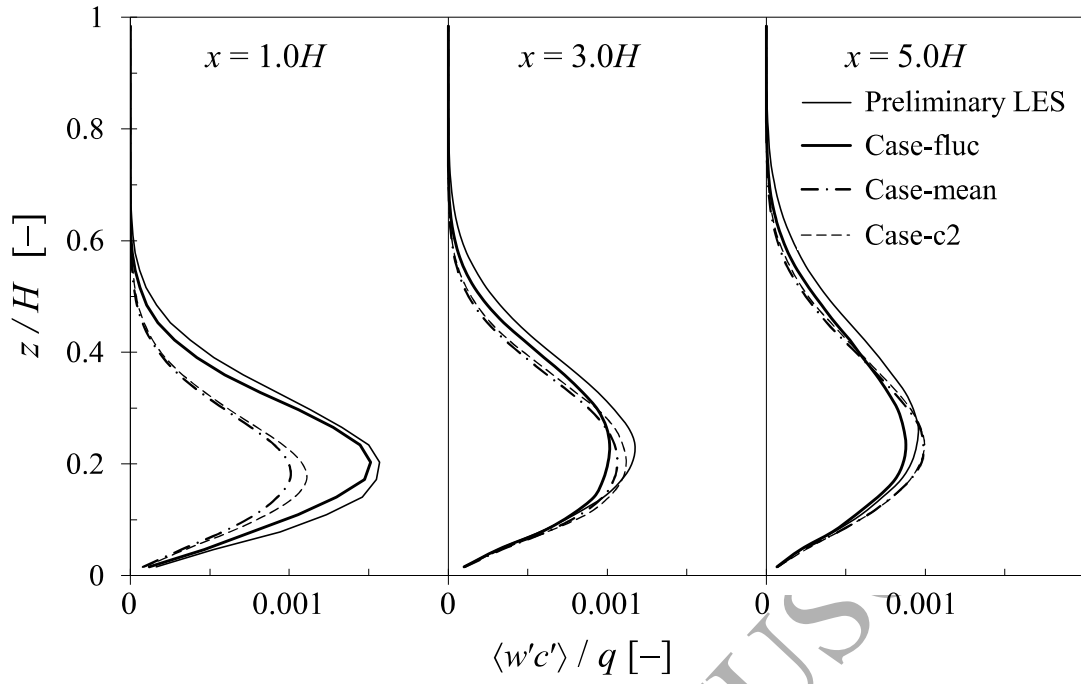Fig. 5 Streamwise change of vertical distribution of mean concentration

Fig. 6 Streamwise change of vertical distributions of turbulence flux of passive scalar for vertical component
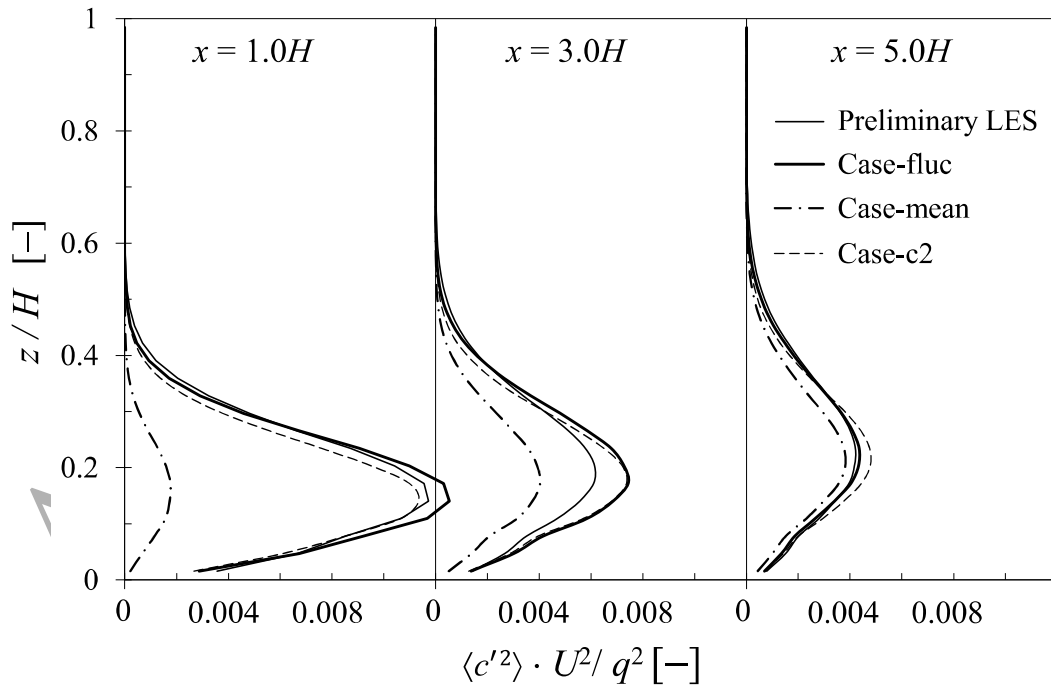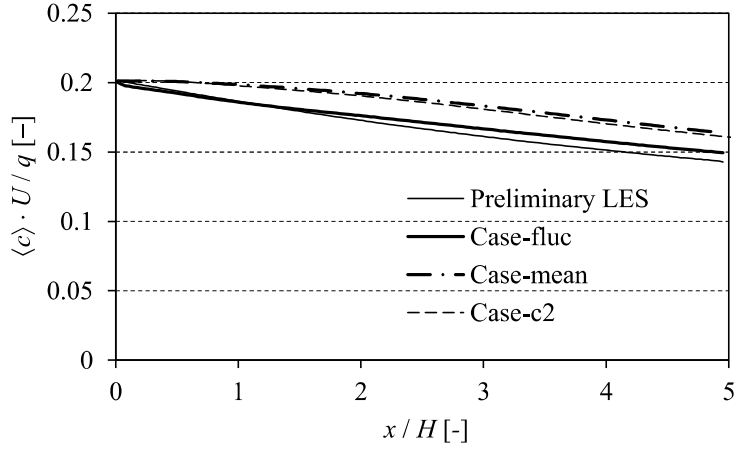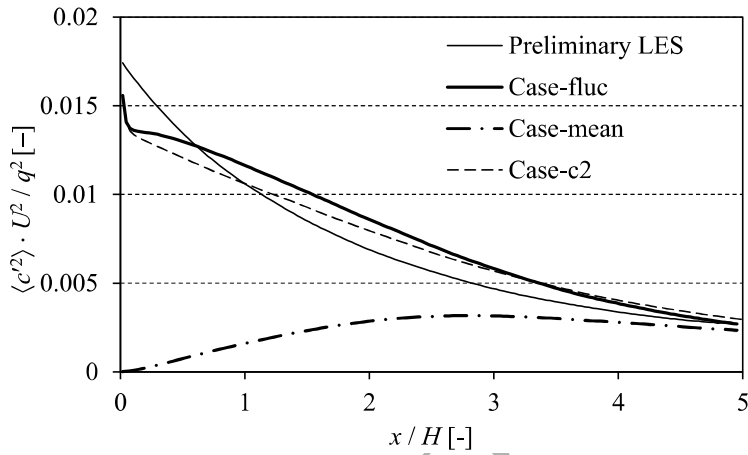

Fig. 7 Streamwise change of vertical distributions of variance of passive scalar fluctuation

(a) Mean concentration

(b) Variance of fluctuation of concentration

Fig. 8 Streamwise changes of the mean concentration and the variance of the fluctuation of

the concentration at $z = 0.1H$

(a) Mean concentration

(b) Variance of fluctuation of concentration

Table 1. Computational cases

Case	Inflow boundary conditions of main simulation
Case-fluc	All components of turbulence fluxes of he momentum and the scalar, R_{ij}, defined in Eq. (4) are considered. $$R_{ij} = \begin{pmatrix} \langle u'u' \rangle & \langle u'v' \rangle & \langle u'w' \rangle & \langle u'c' \rangle \\ \langle v'u' \rangle & \langle v'v' \rangle & \langle v'w' \rangle & \langle v'c' \rangle \\ \langle w'u' \rangle & \langle w'v' \rangle & \langle w'w' \rangle & \langle w'c' \rangle \\ \langle c'u' \rangle & \langle c'v' \rangle & \langle c'w' \rangle & \langle c'c' \rangle \end{pmatrix}$$
Case-mean	The scalar fluctuation was not generated. This means that the cross-correlations of wind and scalar fluctuations and the variance of scalar fluctuaion were set to zero. $$R_{ij} = \begin{pmatrix} \langle u'u' \rangle & \langle u'v' \rangle & \langle u'w' \rangle & 0 \\ \langle v'u' \rangle & \langle v'v' \rangle & \langle v'w' \rangle & 0 \\ \langle w'u' \rangle & \langle w'v' \rangle & \langle w'w' \rangle & 0 \\ 0 & 0 & 0 & 0 \end{pmatrix}$$
Case-c2	The scalar fluctuation was generated by only prescribing the variance of scalar fluctuation. The cross-correlations of wind and scalar fluctuaions were set to zero. $$R_{ij} = \begin{pmatrix} \langle u'u' \rangle & \langle u'v' \rangle & \langle u'w' \rangle & 0 \\ \langle v'u' \rangle & \langle v'v' \rangle & \langle v'w' \rangle & 0 \\ \langle w'u' \rangle & \langle w'v' \rangle & \langle w'w' \rangle & 0 \\ 0 & 0 & 0 & \langle c'c' \rangle \end{pmatrix}$$